RSC Advances

PAPER

View Article Online
View Journal | View Issue

Cite this: *RSC Adv.*, 2019, **9**, 6986

A green L-cysteine modified cellulose nanocrystals biosorbent for adsorption of mercury ions from aqueous solutions†

Weixue Li, Benzhi Ju * and Shufen Zhang

Using a green biosorbent to remove toxic mercury ions from aqueous solutions is a significant undertaking. In the present study, a novel biosorbent, L-cysteine modified cellulose nanocrystals (Lcys-CNCs), was prepared by functionalizing high surface area cellulose nanocrystals with L-cysteine through periodate oxidation and reductive amination reaction. Lcys-CNCs were characterized by FT-IR, ^{13}C CP-MAS NMR, elemental analysis, XPS, zeta potential and SEM. As cellulose nanocrystals are the natural nanomaterial, and L-cysteine contains strong mercury chelating groups, Lcys-CNCs show excellent adsorption capacity for mercury ions. The experimental conditions such as pH, contact time, and initial mercury ion concentration are discussed. The pseudo-second order model can describe the removal kinetics of Hg(II) more accurately than the pseudo-first order model. The adsorption isotherm study of Hg(II) followed the Langmuir model of monolayer adsorption. The maximum uptake capacity of Lcys-CNCs was determined to be 923 mg g^{-1}. Lcys-CNCs can remove mercury ions with 93% removal efficiency within 5 min from a 71 mg L^{-1} solution. For Cd(II), Pb(II), Cu(II) and Zn(II) ions, Lcsy-CNCs can selectively adsorb Hg(II) ions and the removal efficiency is 87.4% for Hg(II). This study suggests Lcsy-CNCs are a green and highly efficient biosorbent for adsorption of mercury ions from aqueous solutions.

Received 3rd January 2019
Accepted 12th February 2019

DOI: 10.1039/c9ra00048h

rsc.li/rsc-advances

1. Introduction

Mercury is a common heavy metal that is toxic to living organisms. In recent decades, the development of modern industry has caused mercury pollution to a great extent.[1,2] The accumulation of mercury in human bodies can cause serious health issues.[3] Therefore, the removal of Hg(II) pollutants from water is required to reduce the harm of Hg(II) to organisms.[4] Among various treatment methods, adsorption is an effective, simple and feasible method to remove Hg(II) from water.[5] At present, many adsorbents (such as inorganic[6–8] and organic materials[9]) have been developed to remove Hg(II) from aqueous solutions. However, their application is limited because they are not renewable or cause secondary pollution to the environment. According to the concept of sustainable development, it is important to develop a green biosorbent[10] based on biomass that can efficiently and selectively remove mercury ions. Biosorbents are more favored than traditional adsorbents, due to their less toxicity, wide sources and biodegradation.[11,12] Commonly used biosorbents include cellulose-based adsorbents,[13–15] chitosan-based adsorbents,[16,17] and *Agaricus macrospores*,[18] *etc.* However, these reported biosorbents still face many challenges such as low specific surface area, less mercury chelating groups and poor selective adsorption of mercury ions.

Cellulose is the most abundant biopolymer in nature. And its nanoform, cellulose nanocrystals (CNCs), can be used as a promising adsorbent due to their sustainability, biodegradability, biocompatibility and high specific surface properties.[19] However, the adsorption capacity of CNCs is not high due to the lack of strong mercury chelating groups.

The introduction of functional groups (*e.g.* amino group, thiol group) that have strong affinity to Hg(II) ions on the surface of adsorbents can improve their adsorption capacity for mercury ions.[20] Liu and co-workers[21] reported that maximum adsorption capacity was 718 mg g^{-1} by 3-mercaptopropyltrimethoxysilane (MPTs) modified TO-NFC aerogel. Zhang and co-workers[22] reported that the maximal uptake capacity as high as 543 mg g^{-1} by triethylenetetramine (TETA) functionalized magnetic poly(glycidyl methacrylate) (PGMA) nano-adsorbent. Therefore, increasing the content of amino and thiol group on the CNC can help increase its adsorbability of mercury ions.

L-Cysteine is a common amino acid in the body, and contains strong mercury chelating groups such as thiol group, amino group. The L-cystine functionalized-exfoliated graphene oxide adsorbent have been used for removal of Hg(II).[23] L-Cysteine doped polypyrrole (PPy@L-Cyst) have been reported to be rapid and efficient removal of Hg(II) ions from water.[24] Thus, the content of the thiol group and the amino group on the surface of the CNCs is increased by grafting L-cysteine.

State Key Laboratory of Fine Chemicals, Dalian University of Technology, Dalian 116024, PR China. E-mail: jubenzhi@dlut.edu.cn; Fax: +86 411 84986264; Tel: +86 411 84986269

† Electronic supplementary information (ESI) available. See DOI: 10.1039/c9ra00048h

In this study, a green biosorbent, L-cysteine modified cellulose nanocrystals, was successfully synthesized by periodate oxidation and reductive amination reaction. Lcys-CNCs have the following features: renewability because the raw material is green biomass; high specific surface; a large number of mercury chelating groups (thiol and amino groups) that are anchored to CNCs by covalent bond. The effect of pH, contact time, mercury ions initial concentration was thoroughly investigated to optimize the adsorption process. Herein, Lcys-CNCs exhibited the excellent adsorption capacity for mercury ions and could quickly achieve adsorption equilibrium. Lcys-CNCs can selectively adsorb mercury ions in the presence of other coexisting metal ions, and show a good regeneration performance.

2. Experimental

2.1 Chemicals and reagents

Qualitative filter paper (Hangzhou Fuyang Special Paper Industry Co., Ltd.) were used as CNC source. Sulfuric acid (H_2SO_4, 98%), sodium periodate ($NaIO_4$), glycol, L-cysteine and sodium cyanoborohydride ($NaBH_3CN$) were purchased from Sigma-Aldrich.

2.2 Synthesis of dialdehyde cellulose nanocrystal

CNCs were synthesis by H_2SO_4 hydrolysis of filter paper. The powdered filter paper was added slowly into sulfuric acid (64 wt%, 10 mL g^{-1}) under mechanical stirring at 45 °C for 45 min, then deionized water (4 °C, 10 equivalents per mL of the reaction solution) was added into reaction. CNCs were separated from the resulting suspension by centrifugation (9000 rpm, 5 min). The sediment was dialyzed with the dialysis membranes (molecular weight cut-off, MWCO: 8000–14 000) against deionized water to neutrality. Then the suspension could remove aggregates by centrifugation (8000 rpm, 10 min). The CNC suspension (2.0 wt%) and sodium periodate (corresponding to 6.0 mmol g^{-1} CNCs) were mixed for 12 h in the absence of light at 40 °C. At the end the oxidation period, 10 mL ethylene glycol was added into the reaction mixture to remove the residual sodium periodate. The resulting product was dialyzed (MWCO: 8000–14 000) against deionized water to that of deionized water (~5 μS cm^{-1}). The resulting dialdehyde cellulose (DAC) nanocrystal was stored at 5 °C.[25,26]

The aldehyde content of DAC was measured by the Schiff base reaction between aldehyde groups and hydroxylamine hydrochloride.[27,28] In this work, aldehyde content of DAC was 3.49 mmol g^{-1}.

2.3 Synthesis of Lcys-CNCs

L-Cysteine (9.51 g) was slowly added to DAC (300 mL, 0.015 g mL^{-1}) suspension, then the reaction was stirred for 6 h at room temperature. $NaBH_3CN$ (1.97 g) was added in multiple steps into reaction and continued for 6 h at room temperature, followed by addition of HCl dilute solution (3 mol L^{-1}) to neutralize the excess $NaBH_3CN$. The resulting product was dialyzed (MWCO: 8000–14 000) against deionized water to that of deionized water (~5 μS cm^{-1}), then freeze dried.

2.4 Characterization

Characterization is shown in ESI.†

2.5 Adsorption/desorption studies

Batch adsorption experiments were conducted by a certain amount of dry Lcys-CNCs (~10 mg) were added into 30 mL Hg(II) solution, at different Hg(II) concentration (71–502 mg L^{-1}) and contact time (0.5–180 min), the varying pH value (2–7), and constant 25 °C.[29] Afterwards, the precipitate was separated by centrifugation (5000 rpm, 10 min) and the amount of mercury in the solution was quantified by ICP-MS. In addition, the selective removal of Hg(II) from a solution containing Hg(II) at 116 mg L^{-1} and other toxic metals Pb(II), Cd(II), Zn(II) and Cu(II) at 90, 80, 108 and 91 mg L^{-1}, respectively, was evaluated at pH 5 and 25 °C for 3 h. Desorption was carried out using Lcys-CNCs preloaded with Hg(II) in mercury ion solution. Briefly, a known amount of the loaded Lcys-CNCs were eluted with 2 M HCl and 0.5 M thiourea by stirring for 30 min at 25 °C. For the regeneration study of Lcys-CNCs, this adsorption–desorption cycle was repeated four times. The amount of mercury adsorbed per gram and removal efficiency of Lcys-CNCs was calculated according to following equations.[30,31]

$$Q_e = \frac{(C_o - C_e)V}{m} \quad (1)$$

$$\text{Removal efficiency} = \frac{C_o - C_e}{C_o} \times 100\% \quad (2)$$

where Q_e is the adsorption capacity of Lcys-CNCs (mg g^{-1}) at equilibrium, C_o is the initial concentration of mercury (mg L^{-1}), C_e is in the concentration of the mercury ion (mg L^{-1}) at equilibrium, V is the volume of the solution (L), and m is the weight of Lcys-CNCs (g).

3. Results and discussion

3.1 Synthesis and characterization

CNCs were prepared by H_2SO_4 (64 wt%) hydrolysis from filter paper after which rod-shaped crystalline region (CNC) remained while the amorphous region was removed. Sodium periodate could selectively oxidize CNC and cleave the C2–C3 bond to synthesize DAC. DAC was then grafted with L-cysteine to obtain Lcys-CNCs through reductive amination reaction (Scheme 1).

The molecular structure of Lcsy-CNCs was determined by FT-IR, XPS and solid-state ^{13}C NMR. The FT-IR spectra of CNCs, DAC and Lcsy-CNCs was shown in Fig. 1A. As shown in Fig. 1A, CNCs, DAC and Lcys-CNCs had the same absorption bands at 3418, 1634, 1436, 1318, 1164 and 665 cm^{-1} correspond to the OH stretching vibration, OH bending vibration of absorbed water, the HCH and OCH in-plane bending vibration, CH_2 rocking vibration at the C_6 position, C–O–C asymmetrical stretching and C–OH out-of-plane bending, respectively.[32] These absorption bands indicate that the CNCs, DAC and Lcys-CNCs have characteristic bands of cellulose. Compared to CNCs, the characteristic absorption band appeared at 1730 cm^{-1} for the stretching vibration of the C=O of DAC,

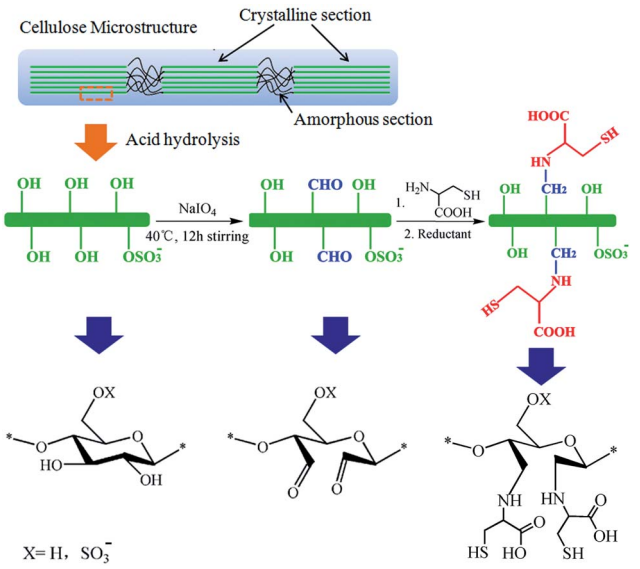

Scheme 1 Oxidation and reduction reaction of cellulose nanocrystals.

which is caused by the formation of aldehyde groups. The two absorption bands at 1731 and 2550 cm^{-1} in the spectrum of Lcys-CNCs correspond to COOH and S–H groups, respectively. This result indicated that L-cysteine was grafted onto CNCs surface.

XPS was used to further study the surface chemical composition of Lcsy-CNCs. As shown in Fig. 1B, compared to CNCs, Lcys-CNCs shown new peaks appeared in the N 1s and S 2p regions. The S 2p XPS spectrum of Lcsy-CNCs (Fig. 1C, Table S1†) displayed two characteristic peaks, one of which for sulfate (high oxidation state sulfur, S 2p 3/2 at 167.0 eV and S 2p 1/2 at 168.4 eV) and the other for thiol groups (S 2p 3/2 at 161.6 eV and S 2p 1/2 at 162.8 eV).[33] At the same time, the N 1s XPS spectrum of Lcsy-CNCs (Fig. 1D) shown two characteristic peaks, one of which (397.8 eV) was assigned to amino groups and one of which (400.1 eV) was assigned to the protonatable amino groups (amino groups were protonated when HCl was added to remove unreacted $NaBH_3CN$). The C 1s XPS spectrum of Lcsy-CNCs (Fig. 1E) shown four peaks, which were attributed to C–C (283.8 eV), C–O (284.7 eV), O–C–O (286.0 eV) and O–C=O (286.8 eV), respectively. Moreover, the O 1s XPS spectrum of Lcsy-CNC (Fig. 1F) displayed two splitting peaks of the binding energy at 530.0 and 531.1 eV could be assigned to C–O–H and O–C–O or C=O.[34]

The structure of Lcys-CNCs was also analyzed with the solid-state ^{13}C NMR. As can be seen in Fig. 1G–H, the ^{13}C CP-MAS NMR spectra of CNCs and Lcys-CNCs displayed typical signals from cellulose, C1 (105 ppm), C2, C3 and C5 (70–80 ppm), C4 (~89 ppm), and C6 (~65 ppm).[35,36] Moreover, ^{13}C CP-MAS NMR spectra of Lcys-CNCs (Fig. 1H) showed peaks at 32 ppm (C8 carbons, –C–S) 54 ppm (C7 carbons, –C–N) and 174 ppm (C9 carbons, –C=O).[37,38]

The contents of surface S and N of the adsorbent directly affect its adsorption capacity of Hg(II).[21] The proportions of S and N in CNCs and Lcys-CNCs are performed by elemental analysis in Table 1. The calculated content of surface S and N elements in Lcys-CNCs was 2.80 and 2.77 mmol g^{-1}, respectively. Therefore, the nitrogen and sulfur contents of Lcys-CNCs were significantly increased after CNCs modification by L-cysteine. The specific surface area of adsorbent is also a major factor affecting the adsorption performance. The N_2 adsorption–desorption isotherms of CNCs and Lcys-CNCs are presented in Fig. S1.† The BET specific surface area of CNCs and Lcys-CNCs shown in the Table 1, reveal that Lcys-CNCs (72.10 $m^2\ g^{-1}$) have a much higher BET surface area than that of CNCs (10.81 $m^2\ g^{-1}$) due to the destruction of the ordered packing of CNCs by sodium periodate oxidation and post-modification reactions, which loosens its surface.

Thus, the factors affecting the adsorption capacity of mercury ions include specific surface area and mercury chelating groups. Lcys-CNCs are the nano-material with higher specific surface area. A large number of amino and thiol groups were introduced on the surface of CNCs by chemical modification. Therefore, Lcys-CNCs with the above structural characteristics implies it can efficiently adsorb mercury ions.

3.2 Adsorption studies

To evaluate the adsorption capacity of Lcsy-CNCs for removing Hg(II), a certain amount of dry Lcys-CNCs were added into 30 mL Hg(II) solution at 25 °C. The pH value of solution can change the surface charge density of adsorbent, and influences the adsorption property of Hg(II). Therefore, the effect of pH value on the adsorption capacity of Hg(II) by Lcys-CNCs (Fig. 2a) and the effect of zeta potential of Lcys-CNCs at different pH values (Fig. 2b) were studied.

When CNCs were used as adsorbent, the adsorption was very low, and the pH value had a mild influence on the adsorption. However, after the L-cysteine was introduced on CNCs, the adsorption capacity of Hg(II) was greatly increased, and the adsorption capacity also changed at different pH values. When the pH was raised from 2 to 5, the adsorption of mercury ions by Lcys-CNCs showed an upward trend. At pH 5, it reached the maximum, but the adsorption properties decreased with pH value (>5) increased.

The reason why the uptake capacity of Lcys-CNCs was affected by pH is as follows. At pH 1.56, the zeta potential of Lcys-CNCs was +4.39 mV due to the –NH– groups of Lcys-CNCs were protonated. At the same time, the protons compete with Hg(II) ions for getting adsorbed onto active sites of adsorbent and electrostatic repulsion between mercury ions and Lcys-CNCs results in decreasing adsorption of Hg(II).[39] The zeta potential of Lcys-CNCs decreases rapidly with increasing pH value, because the deprotonation of the amine and carboxyl groups on the surface of Lcys-CNC at high pH. At pH 5, L-cysteine reaches the isoelectric point, the number of protonated amino groups and deprotonated carboxyl groups is equal, and L-cysteine is uncharged.[40] However, Lcys-CNC is obtained by introducing L-cysteine into the surface of the CNC, and its surface contains not only amino, carboxyl groups but also sulfate groups. Therefore, the potential of Lcys-CNC is −28.3 mV at pH 5.31, and Lcys-CNC has strong electrostatic attraction to Hg(II) and can quickly, effectively adsorb Hg(II)

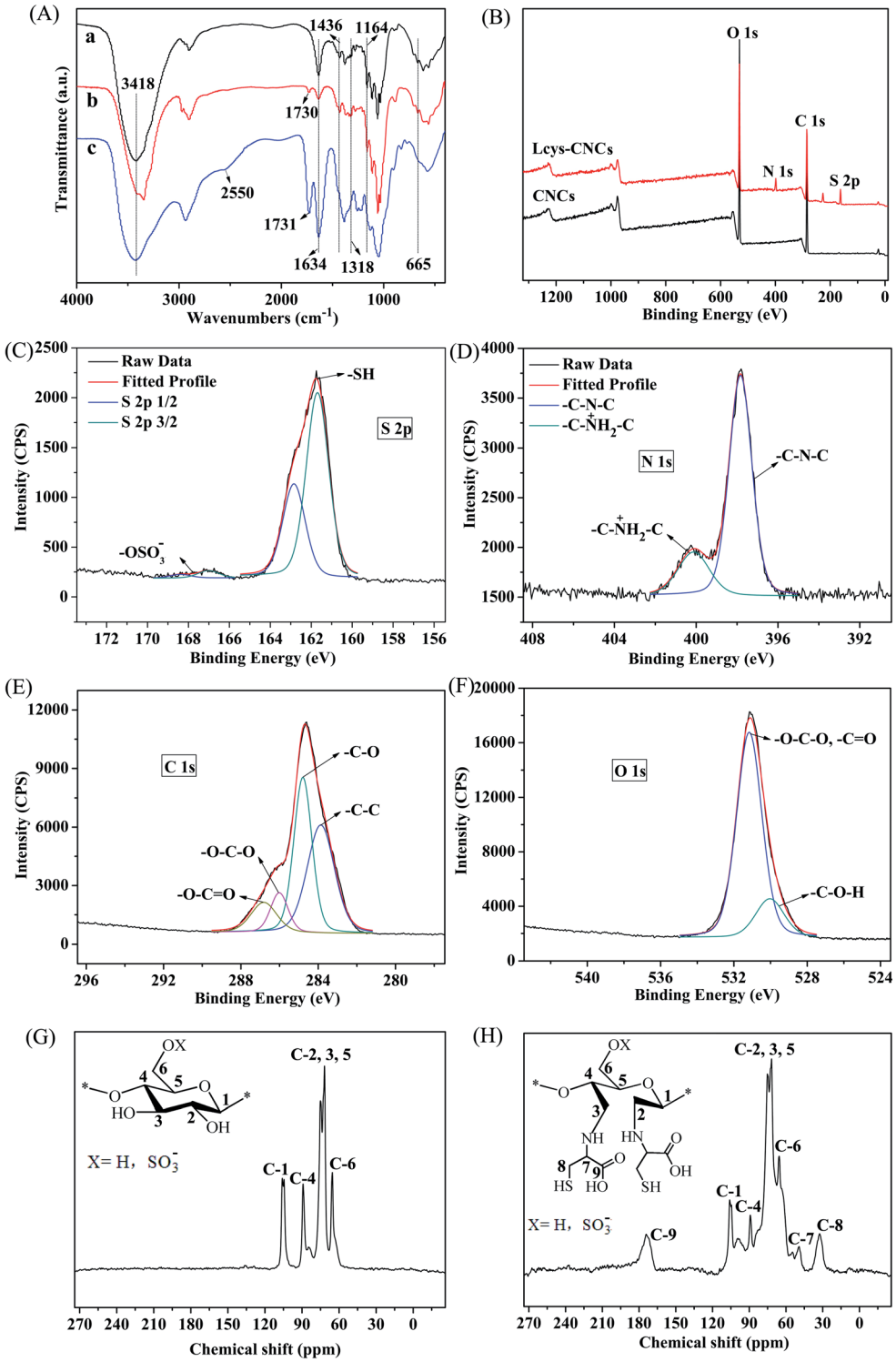

Fig. 1 (A) The FT-IR spectra of CNCs (a), DAC (b) and Lcys-CNCs (c); (B) XPS survey spectra of CNCs and Lcys-CNCs. The S 2p XPS spectrum (C), N 1s XPS spectrum (D), C 1s XPS spectrum (E) and O 1s XPS spectrum (F) of Lcys-CNC; ^{13}C CP-MAS NMR spectra of CNCs (G) and Lcys-CNCs (H).

from aqueous solutions. Lcys-CNCs reach the maximum uptake capacity (587 mg g^{-1}) at pH 5 (Fig. 2a). Although the zeta potential of Lcys-CNCs decreases with pH value (>5) increases, the amount of OH^- increases, and OH^- groups react with Hg(II) ions to form $Hg(OH)^+$, $Hg(OH)_2$, and $Hg(OH)_3^-$, which reduces the adsorption effect.[41]

3.3 Adsorption kinetics

When the adsorbent reached the adsorption equilibrium, the required contact time can evaluate the adsorbent. After Lcys-CNCs were added to the mercury ion solution, the adsorption capacity of mercury ion changed with the contact time.[42] The influence of contact time on the uptake of mercury ions onto

Table 1 Composition of CNCs and Lcys-CNCs measured by elemental analysis; content of surface S element, surface N element and BET surface area of the samples

	Elemental analysis				Surface S	Surface N	BET surface area
Samples	% C	% H	% S	% N	mmol g^{-1}	mmol g^{-1}	m^2 g^{-1}
CNCs	41.36	6.70	0.89	0.29	0.27	0.20	10.81
Lcsy-CNCs	41.85	6.15	8.98	3.89	2.80	2.77	72.10

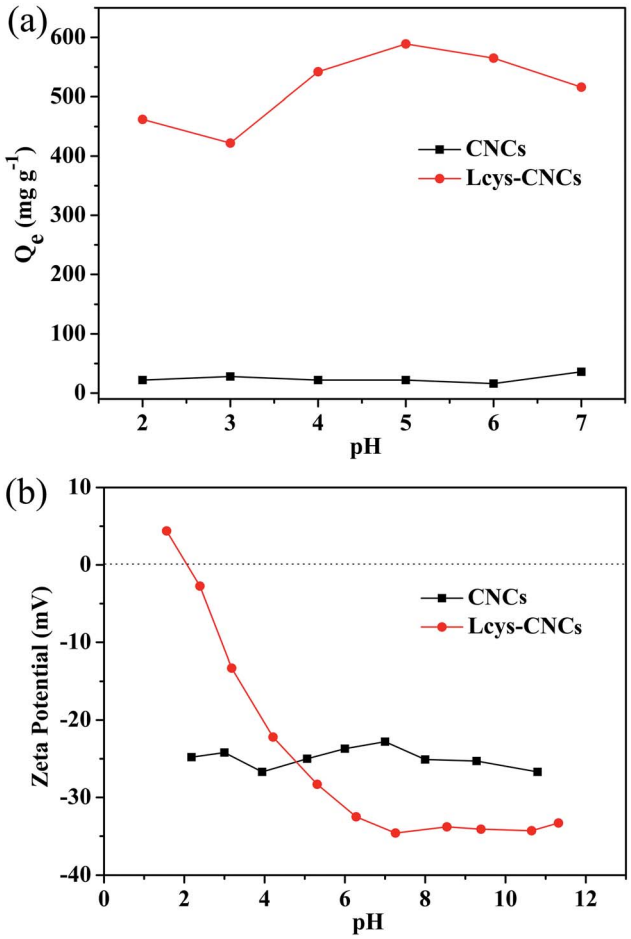

Fig. 2 (a) Effect of pH value on the adsorption capacity of Hg(II) (215 mg L^{-1}, 25 °C, 3 h, pH 2–7). (b) Zeta potential of CNCs and Lcys-CNCs at different pH values (1.0 g L^{-1}, 25 °C, 0.01 M KCl).

Lcys-CNCs (Fig. 3a) was investigated in 30 mL of 71 mg L^{-1} Hg(II) solution (pH 5) at 25 °C. When Lcys-CNCs were added to the mercury ion solution, mercury ions could be quickly and efficiently adsorbed from aqueous solution because of Lcys-CNCs with high specific surface area and a large number of active sites. In particular, the negative charge of Lcys-CNCs could further accelerate the arrival of Hg(II) ions on the surface of the adsorbent by electrostatic interaction.[21] Afterword, the active sites decreased due to mercury ions accumulated on the surface of Lcys-CNCs. Therefore, the adsorption rate gradually slowed down, then achieved adsorption equilibrium within 5 min.

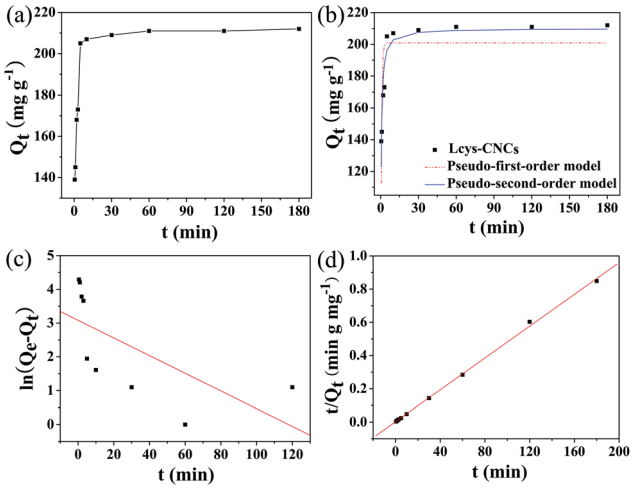

Fig. 3 Effect of contact time on the adsorption capacity of Hg(II) (a); nonlinear forms of pseudo-first-order model and pseudo-second-order model for adsorption of Hg(II) by Lcys-CNCs (b); linear forms of pseudo-first-order model (c) and pseudo-second-order model (d) (71 mg L^{-1}, pH 5, 25 °C, 0.5–180 min).

The adsorption kinetic study can explain the adsorption mechanism. Therefore, pseudo-first-order and pseudo-second-order kinetic models (Fig. 3b–d) were applied to describe the adsorption of mercury ions onto Lcys-CNCs, and their models were shown as the following equations.

Nonlinear forms of pseudo-first-order:

$$Q_t = Q_e[1 - \exp(-k_1 t)] \quad (3)$$

Linear forms of pseudo-first-order:

$$\ln(Q_e - Q_t) = \ln Q_e - k_1 t \quad (4)$$

Nonlinear forms of pseudo-second-order:

$$Q_t = \frac{t}{1/k_2 Q_e^2 + t/Q_e} \quad (5)$$

Linear forms of pseudo-second-order:

$$\frac{t}{Q_t} = \frac{1}{k_2 Q_e^2} + \frac{1}{Q_e} t \quad (6)$$

where Q_e and Q_t are the adsorption capacity (mg g^{-1}) at equilibrium time and at time t (min), k_1 and k_2 are pseudo-first order rate constant (min^{-1}), and pseudo-second order rate constant (g mg^{-1} min^{-1}), respectively.

Table 2 Adsorption kinetics values of Lcys-CNCs for Hg(II)

	Pseudo-first-order						
	Nonlinear form				Linear form		
Sample	Q_e,exp[a] (mg g^{-1})	Q_e,cal[b] (mg g^{-1})	k_1 (min^{-1})	R^2	Q_e,cal (mg g^{-1})	k_1 (min^{-1})	R^2
Lcys-CNCs	211	200	1.649	0.6340	21	2.61×10^{-2}	0.6641

[a] Q_e,exp: experimental adsorption capacity. [b] Q_e,cal: calculated adsorption capacity.

	Pseudo-second-order						
	Nonlinear form				Linear form		
Sample	Q_e,exp (mg g^{-1})	Q_e,cal (mg g^{-1})	k_2 (g mg^{-1} min^{-1})	R^2	Q_e,cal (mg g^{-1})	k_2 (g mg^{-1} min^{-1})	R^2
Lcys-CNCs	211	210	1.34×10^{-2}	0.8947	209	1.08×10^{-2}	0.9994

Adsorption kinetics values of Lcys-CNCs for Hg(II) are summarized in Table 2. The equilibrium adsorption capacity calculated based on the pseudo-second order model is closer to the experimental data than the pseudo-first order model, and correlation coefficients (R^2) value for the pseudo-second order model is much better than the pseudo-first order model. Therefore, the adsorption kinetics was accurately described by a pseudo-second order model, suggesting that the adsorption of Hg(II) on Lcys-CNCs was mainly through chemical reactive adsorption between active sites (thiol group and amino group) of Lcys-CNCs and Hg(II) ions.[43]

3.4 Adsorption isotherm

The initial concentration of mercury ion is also an important factor in affecting the mercury uptake capacity of Lcys-CNCs. The effect of initial ion concentration (71–502 mg L^{-1}) on the adsorption capacity of Hg(II) was shown in Fig. 4a. The adsorption values increased with the enhancing of initial concentration of mercury ion, then attained a platform. The equilibrium adsorption isotherm can help explain the relationship of metal ions and adsorbent molecule. The Langmuir and Freundlich models (Fig. 4b–d) are two well-known isothermal adsorption models, and their models are shown as the following equations.

Nonlinear forms of Langmuir:

$$Q_e = \frac{Q_m b C_e}{1 + b C_e} \quad (7)$$

Linear forms of Langmuir:

$$\frac{C_e}{Q_e} = \frac{1}{b Q_m} + \frac{C_e}{Q_m} \quad (8)$$

Nonlinear forms of Freundlich:

$$Q_e = K_F C_e^{\frac{1}{n}} \quad (9)$$

Linear forms of Freundlich:

$$\ln(Q_e) = \ln(K_F) + \frac{1}{n}\ln(C_e) \quad (10)$$

where C_e, Q_e and Q_m are the equilibrium concentration (mg L^{-1}), the equilibrium adsorption capacity of the adsorbent (mg g^{-1}) and the maximum adsorption capacity (mg g^{-1}), respectively. K_F and b are the Freundlich and Langmuir constant, and n is the heterogeneity factor.

The calculated parameters for Langmuir and Freundlich isotherm models of Lcys-CNCs are summarized in Table 3. The R^2 of Langmuir model are higher than Freundlich model, and the maximum adsorption values calculated by Langmuir model are close to the experimental data (923 mg g^{-1}), and which is higher than most of the adsorbents reported in the literatures (Table 4). Therefore, the equilibrium adsorption isotherm data was fitted with Langmuir model, suggesting that Hg(II) adsorption on adsorbent is a monolayer coverage. For the

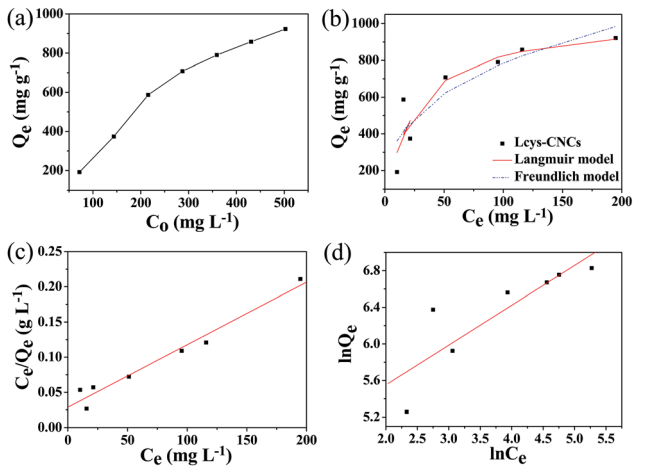

Fig. 4 Effect of initial ion concentration on the adsorption capacity of Hg(II) (a); nonlinear forms of Langmuir isotherm model and Freundlich isotherm model for adsorption of Hg(II) by Lcys-CNCs (b); linear forms of Langmuir isotherm model (c) and Freundlich isotherm model (d) (3 h, pH 5, 25 °C, 71–502 mg L^{-1}).

Table 3 Langmuir and Freundlich values of Lcys-CNCs for Hg(II)

	Langmuir					
	Nonlinear form			Linear form		
Sample	b (L mg^{-1})	Q_m (mg g^{-1})	R^2	b (L mg^{-1})	Q_m (mg g^{-1})	R^2
Lcys-CNCs	3.94×10^{-2}	1034	0.8627	3.11×10^{-2}	1116	0.9818
	Freundlich					
	Nonlinear form			Linear form		
Sample	$1/n$	K_F (mg$^{1-1/n}$ g^{-1} L$^{1/n}$)	R^2	$1/n$	K_F (mg$^{1-1/n}$ g^{-1} L$^{1/n}$)	R^2
Lcys-CNCs	0.34	163.70	0.8179	0.43	107.77	0.8605

Langmuir model, the values of b (0.03–0.04) lie between 0 and 1, indicating a favorable adsorption process.[44]

3.5 Adsorption mechanism

The surface microstructure of Lcys-CNCs was analyzed by SEM (Fig. 5a) and it shown that rodlike shape with length of 228 ± 57 nm and width of 25 ± 6 nm (Fig. S2, Table S2†). Although the morphology of Hg(II)-loaded Lcsy-CNCs (Fig. 5b) was still rodlike shape, there was a accumulation phenomenon, and the width (35 ± 11 nm) was obviously broader due to adsorptions of Hg(II) on the same Lcys-CNCs or between with Lcys-CNCs.[46] It was further proved by EDX spectrum of Hg(II)-loaded Lcsy-CNCs (Fig. 5c) that Lcys-CNCs effectively adsorbed a large amount of mercury ions.

When Lcys-CNCs were added to the mercury ion solution, the proposed mechanism of Hg(II) uptake onto Lcys-CNCs was shown in Fig. 5d. Compared to the common adsorbents, nano-adsorbent Lcys-CNCs have higher specific surface area (72.10 m^2 g^{-1}). The high specific surface area of Lcys-CNCs is beneficial to contact with more mercury ions. Moreover, the negative charge of Lcys-CNCs could further accelerate the arrival of mercury ions on the surface of the adsorbent by electrostatic interaction. Then, the lone pairs of electrons of the S, N and O elements on the Lcys-CNCs could rapidly complex mercury ions. The abundant active groups (amino and thiol groups) of Lcys-CNCs indicate that it has the excellent adsorption capacity. Therefore, Lcsy-CNCs could rapidly and efficiently adsorb mercury ions from aqueous solution, through complexation and electrostatic attraction.

Table 4 Comparison of adsorption capacity with other reported adsorbents

Adsorbent	Q_{max} (mg g^{-1})	Ref.
TO–NFC–Si–SH	718	38
P(MB-IA)-*g*-MNCC	240	45
Guanyl-modified celluloseI	48	14
Mercaptobenzothiazole impregnated cellulose	204	20
Lcys-CNCs	923	This work

3.6 Selective studies

In contaminated water, mercury ions often coexist with a large number of other metal ions. The adsorption capacity of mercury ion can also be affected by the presence of other coexisting metal ions. In order to investigate the selectivity of Lcsy-CNCs for mercury ions, Pb(II), Cd(II), Zn(II) and Cu(II) were used as coexisting ions to investigate their effects on the adsorption capacity of mercury ions, as shown in Fig. 6a. The adsorption efficiency of Lcsy-CNCs is 87.4, 2.1, 18.9, 6.1 and 2.7% for Hg(II), Cd(II), Pb(II), Cu(II) and Zn(II), respectively. For the other four kinds of metal ion species, Lcsy-CNCs can selectly adsorb mercury ions. This is mainly based on the Hard-Soft Acid-Base (HSAB) theory, mercury ion was soft acids, and thiol group of Lcsy-CNCs was soft base, mercury ions could form steady complex with thiol groups.[47] Therefore, Lcys-CNCs would

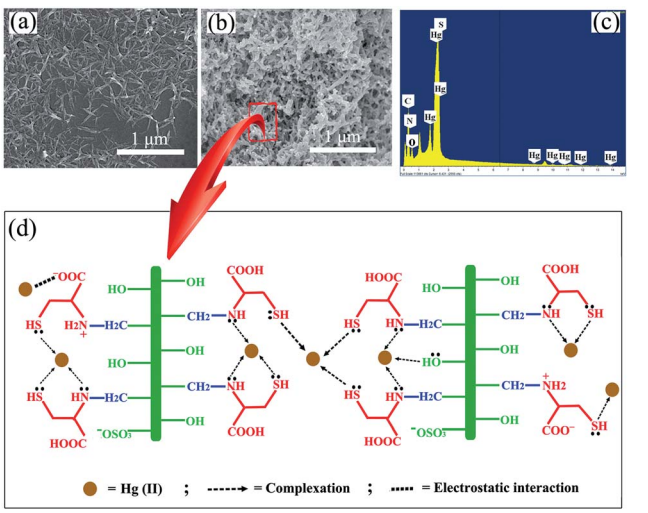

Fig. 5 SEM images of Lcsy-CNCs (a), and Hg(II)-loaded Lcsy-CNCs (b). (c) EDX spectrum of Hg(II)-loaded Lcsy-CNCs. (d) Illustration of the proposed interaction between Lcsy-CNCs and Hg(II).

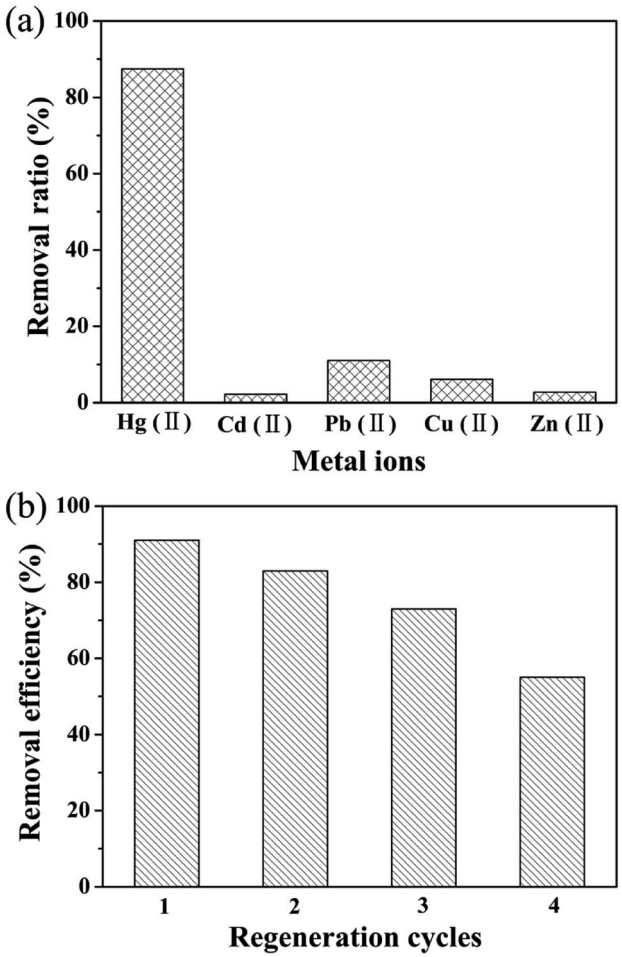

Fig. 6 (a) Selective adsorption results for mercury ions (3 h, pH 5, 25 °C); (b) reusability results for Lcsy-CNCs in Hg(II) solutions (3 h, pH 5, 25 °C).

preferentially and more stably bind Hg(II) relative to other metal ions.

3.7 Reusability test

In practical applications, it is very necessary to investigate the regeneration performance of the adsorbent. The regeneration performance of Lcsy-CNCs was shown in Fig. 6b. After three cycles, the removal percentage of Hg(II) could still keep above 70%, but after the fourth cycle, the removal percentage of Hg(II) for Lcsy-CNCs was reduced to 55%.

4. Conclusions

A green biosorbent, L-cysteine modified cellulose nanocrystals (Lcys-CNCs), was successfully synthesized and applied to adsorb mercury ions from aqueous solutions. Lcys-CNCs show the excellent adsorption capacity for mercury ions. In the mercury ion solution with a concentration of 71 mg L^{-1}, the adsorption of Hg(II) achieved adsorption equilibrium within 5 min. The optimum pH value for Hg(II) removal was 5. The adsorption of Hg(II) fitted Langmuir isotherm and pseudo-second order. The maximum adsorption value of Lcys-CNCs was up to 923 mg g^{-1}. And Lcys-CNCs can selectively adsorb mercury ions in the presence of other coexisting metal ions. After three adsorption/desorption cycles, the removal percentage of Hg(II) could still keep above 70%. Therefore, Lcsy-CNCs have great potential as a green biosorbent for highly efficient adsorption of mercury ions from aqueous solutions.

Conflicts of interest

There are no conflicts to declare.

Acknowledgements

This work was supported by the National Natural Science Foundation of China (Grant No. 21376041), (Grant No. 21076033), (Grant No. 21536002), (Grant No. 21878036).

References

1 N. Lubick and D. Malakoff, *Science*, 2013, **341**, 1443–1445.
2 V. K. Gupta, I. Ali, T. A. Saleh, A. Nayak and S. Agarwal, *RSC Adv.*, 2012, **2**, 6380–6388.
3 P. M. Bolger and B. A. Schwetz, *N. Engl. J. Med.*, 2002, **347**, 1735–1736.
4 T. A. Saleh, *Desalin. Water Treat.*, 2016, **57**, 10730–10744.
5 H. A. Sani, M. B. Ahmad and T. A. Saleh, *RSC Adv.*, 2016, **6**, 108819–108827.
6 C. P. Huang and D. W. Blankenship, *Water Res.*, 1984, **18**, 37–46.
7 G. Blanchard, M. Maunaye and G. Martin, *Water Res.*, 1984, **18**, 1501–1507.
8 N. L. D. Filho, W. L. Polito and Y. Gushikem, *Talanta*, 1995, **42**, 1031–1036.
9 F. Abadast, A. Mouradzadegun and M. R. Ganjali, *New J. Chem.*, 2017, **41**, 5458–5466.
10 U. Farooq, J. A. Kozinski, M. A. Khan and M. Athar, *Bioresour. Technol.*, 2010, **101**, 5043–5053.
11 N. Salamun, S. Triwahyono, A. A. Jalil, T. Matsuura and N. F. M. Salleh, *RSC Adv.*, 2015, **5**, 14129–14137.
12 C. Hou, D. Zhao, S. Zhang and Y. Wang, *Colloid Polym. Sci.*, 2018, **296**, 547–555.
13 S. Kumari and G. S. Chauhan, *ACS Appl. Mater. Interfaces*, 2014, **6**, 5908–5917.
14 I. M. M. Kenawy, M. A. H. Hafez, M. A. Ismail and M. A. Hashem, *Int. J. Biol. Macromol.*, 2018, **107**, 1538–1549.
15 Y. Zhou, X. Hu, M. Zhang, X. Zhuo and J. Niu, *Ind. Eng. Chem. Res.*, 2013, **52**, 876–884.
16 J. D. Merrifield, W. G. Davids, J. D. Macrae and A. Amirbahman, *Water Res.*, 2004, **38**, 3132–3138.
17 J. Song, H. Oh, H. Kong and J. Jang, *J. Hazard. Mater.*, 2011, **187**, 311–317.
18 M. J. Melgar, J. Alonso and M. A. Garcia, *Sci. Total Environ.*, 2007, **385**, 12–19.
19 T. G. M. V. De Ven and A. Sheikhi, *Nanoscale*, 2016, **8**, 15101–15114.

20 A. S. K. Kumar, S. Kalidhasan, V. Rajesh and N. Rajesh, *Ind. Eng. Chem. Res.*, 2013, **52**, 11838–11849.
21 B. Geng, H. Wang, S. Wu, J. Ru, C. Tong, Y. Chen, H. Liu, S. Wu and X. Liu, *ACS Sustainable Chem. Eng.*, 2017, **5**, 11715–11726.
22 Y. Wang, Y. Zhang, C. Hou, X. He and M. Liu, *J. Taiwan Inst. Chem. Eng.*, 2016, **58**, 283–289.
23 A. S. K. Kumar and S. Jiang, *RSC Adv.*, 2015, **5**, 6294–6304.
24 N. Ballav, R. Das, S. Giri, A. M. Muliwa, K. Pillay and A. Maity, *Chem. Eng. J.*, 2018, **345**, 621–630.
25 L. Jin, W. Li, Q. Xu and Q. Sun, *Cellulose*, 2015, **22**, 2443–2456.
26 S. M. A. S. Keshk, A. M. Ramadan and S. Bondock, *Carbohydr. Polym.*, 2015, **127**, 246–251.
27 U. Kim, M. Wada and S. Kuga, *Carbohydr. Polym.*, 2004, **56**, 7–10.
28 F. Azzam, M. Galliot, J. L. Putaux, L. Heux and B. Jean, *Cellulose*, 2015, **22**, 3701–3714.
29 S. Ravi, P. Puthiaraj, K. H. Row, D. Park and W. Ahn, *Ind. Eng. Chem. Res.*, 2017, **56**, 10174–10182.
30 N. M. Bandaru, N. Reta, H. Dalal, A. V. Ellis, J. G. Shapter and N. H. Voelcker, *J. Hazard. Mater.*, 2013, **261**, 534–541.
31 A. Gupta, S. R. Vidyarthi and N. Sankararamakrishnan, *J. Hazard. Mater.*, 2014, **274**, 132–144.
32 S. Y. Oh, D. I. Yoo, Y. Shin and G. Seo, *Carbohydr. Res.*, 2005, **340**, 417–428.
33 A. R. Lokanathan, A. Nykanen, J. Seitsonen, L. Johansson, J. M. Campbell, O. J. Rojas, O. Ikkala and J. Laine, *Biomacromolecules*, 2013, **14**, 2807–2813.
34 L. Tang, T. Li, S. Zhuang, Q. Lu, P. Li and B. Huang, *ACS Sustainable Chem. Eng.*, 2016, **4**, 4842–4849.
35 H. Kono, S. Yunoki, T. Shikano, M. Fujiwara, T. Erata and M. Takai, *J. Am. Chem. Soc.*, 2002, **124**, 7506–7511.
36 M. M. Ibrahim, W. K. Elzawawy and M. A. Nassar, *Carbohydr. Polym.*, 2010, **79**, 694–699.
37 H. Yang and T. G. M. V. De Ven, *Cellulose*, 2016, **23**, 1791–1801.
38 B. Ram and G. S. Chauhan, *Chem. Eng. J.*, 2018, **331**, 587–596.
39 W. R. Knocke and L. H. Hemphill, *Water Res.*, 1981, **15**, 275–282.
40 T. Dashman and G. Stotzky, *Soil Biol. Biochem.*, 1982, **14**, 447–456.
41 M. Arshadi, A. R. Faraji and M. J. Amiri, *Chem. Eng. J.*, 2015, **266**, 345–355.
42 R. Soury, M. Jabli, T. A. Saleh, W. S. AbdulHassan, E. SaintAman, F. Loiseau, C. Philouze and H. Nasri, *RSC Adv.*, 2018, **8**, 20143–20156.
43 E. Repo, J. K. Warchol, T. A. Kurniawan and M. Sillanpaa, *Chem. Eng. J.*, 2010, **161**, 73–82.
44 V. Vadivelan and K. V. Kumar, *J. Colloid Interface Sci.*, 2005, **286**, 90–100.
45 T. S. Anirudhan and F. Shainy, *J. Colloid Interface Sci.*, 2015, **456**, 22–31.
46 H. Dong, J. F. Snyder, K. S. Williams and J. W. Andzelm, *Biomacromolecules*, 2013, **14**, 3338–3345.
47 R. G. Pearson, *J. Chem. Educ.*, 1968, **45**, 581–587.